Front. Phys., 2014, 9(5): 665–670
DOI 10.1007/s11467-014-0434-0

RESEARCH ARTICLE

Modulation of four-wave mixing via photonic band gap

Zhen-Kun Wu[1,†], **Kai-Ge Chang**[1], **Yi Hu**[2], **Yun-Zhe Zhang**[3], **Zi-Hai Jiang**[1], **Yan-Peng Zhang**[1]

[1] *Key Laboratory for Physical Electronics and Devices of the Ministry of Education & Shaanxi Key Lab of Information Photonic Technique and School of Science, Xi'an Jiaotong University, Xi'an 710049, China*

[2] *Education Institute of Taiyuan University, Taiyuan 030001, China*

[3] *Institute of Applied Physics, Xi'an University of Arts and Science, Xi'an 710065, China*

Corresponding author. E-mail: [†]*wuzk1121@163.com*

Received April 28, 2014; accepted June 8, 2014

The dressed four-wave mixing (FWM) in a four-level ^{85}Rb atomic system, experimentally demonstrated in this paper, is comprised by two coexisting processes. One is emission signal due to enhanced nonlinear via electromagnetically induced transparency (EIT). The other is the Bragg reflection of probe beam because of the created photonic band gap (PBG), which is affected by both linear and third-order nonlinear susceptibility. Moreover, we have demonstrated that different experimental parameters can significantly influence the measured signal with flexibly controlled PBG. These studies are found useful for understanding the fundamental mechanisms in generated FWM processing.

Keywords four-wave mixing (FWM), electromagnetically induced transparency (EIT), photonic band gap (PBG)

PACS numbers 42.50.Gy, 42.65.An, 42.70.Qs

1 Introduction

In the past several years, electromagnetically induced transparency (EIT) in atomic medium has attracted worldwide attention [1–6]. In EIT condition, the linear and nonlinear optical properties of the atomic medium are significantly modified. This enables the high-order nonlinear optical process in atomic medium, where the weak optical field is generated and propagates with little linear absorption [1–3]. The enhanced four wave mixing (FWM) process in EIT due to atomic coherence has been experimentally observed in multilevel atomic systems [5, 6]. Besides, a variety of interesting FWM signals are reported due to the periodic atomic coherence induced by standing waves (SWs) [7, 8]. This is also well known as electromagnetically induced grating (EIG) [9–11], which can play an important role in lasing without inversion [12], slow light generation [13], photon controlling and information storage [14], fiber lasers [15], etc. EIG possesses photonic band gap (PBG) that can reflect the probe field [16].

In this paper, we have simultaneously observed the probe transmission, FWM and fluoresce signals with dressing effects in four-level atomic system. We also put much effort on the PBG investigations in EIT atomic vapors, in which the incident beam is only able to "ravel" if it is eigenvalue falls within an allowed band (Floquet-Bloch modes). We have demonstrated that two coexisting signals are in the emission direction of FWM signals. One is the emission signal in the FWM process due to enhanced nonlinear in an opened EIT window of four-level ^{85}Rb atomic system, and the other is the reflection of the probe beam due to created PBG including both linear susceptibility $\chi^{(1)}$ and nonlinear susceptibility $\chi^{(3)}$. Based on this, we have also researched the influence brought by the concomitant PBG of EIG. The organization of the paper is that we briefly introduced theoretical model and experimental setup in Section 2; we display the experimental results and the discussion in detail in Section 3, and in Section 4 we conclude the paper.

2 Theoretical model and experimental setup

Our experiment is implemented in a rubidium atomic vapor. The temperature of the atomic vapor cell is set at 60°C. The relevant energy levels for ^{85}Rb atoms are shown in Fig. 1(a), where levels $|0\rangle(5S_{1/2})$, $|3\rangle(5S_{1/2})$, $|1\rangle(5P_{3/2})$ and $|2\rangle(5D_{3/2})$ form an inversed Y-type system. The continuous laser beams are aligned spatially as

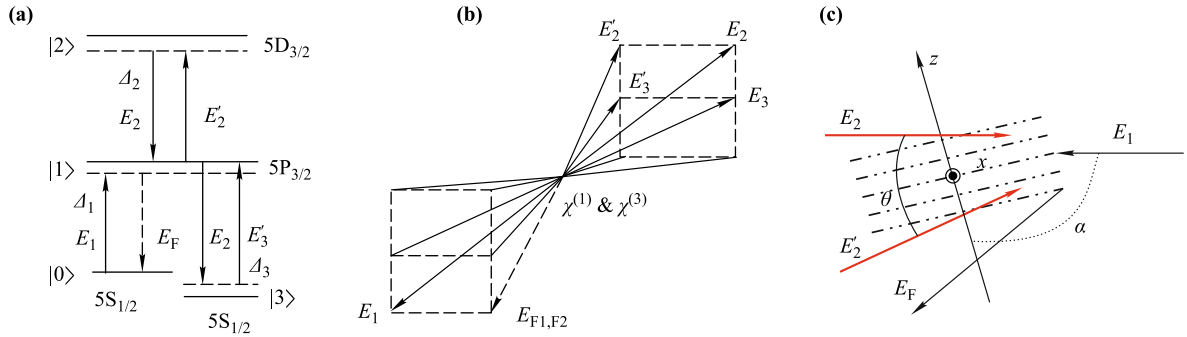

Fig. 1 **(a)** The diagram of relevant ^{85}Rb energy levels. **(b)** Spatial beam geometry. **(c)** Electromagnetically induced grating results from the interference between fields E_2 and E_2'. E_1 is the probe filed and E_F is the reflecting filed.

shown in Fig. 1(b). As displayed in Fig. 1(a), the weak probe beam E_1 with wavevector $\boldsymbol{k}_1$ (with wavelength 780 nm, the power P_1, frequency ω_1, probing the transition $|0\rangle$ to $|1\rangle$ with the atomic resonant frequency Ω_1) from an external cavity diode laser (ECDL), is horizontally polarized and propagate in the opposite direction to the two coupling beam E_3 and E_3' respectively characterized by wavevectors $\boldsymbol{k}_3$ and $\boldsymbol{k}_3'$ (780 nm, P_3, ω_3, driving the transition $|1\rangle$ to $|3\rangle$ with resonant frequency Ω_3) splitting from an ECDL with vertical polarization. Two other pumping beams E_2 and E_2' ($\boldsymbol{k}_2$ and $\boldsymbol{k}_2'$, 776 nm, P_2 and P_2', ω_2, connecting the transition $|1\rangle$ to $|2\rangle$ with resonant frequency Ω_2) are split from a CW Ti:sapphire laser with vertical polarization and also propagate along the opposite direction of E_1 with small angles ($\sim 0.3^\circ$) between them. The pumping beams E_2 and E_2' interfere with each other to induce a vertically aligned grating EIG, which lead to the reflection of the incident probe beam E_1, as shown in Fig. 1(c), where the incident beam E_1 launches obliquely into the grating with angle α. We define the frequency detuning as $\Delta_i = \Omega_i - \omega_i$ $(i = 1, 2, 3)$. Because E_2 counter-propagate with E_1, the Doppler effect can be eliminated near the two-photon resonance. Using this experiment setup, we will investigate three kinds of signals simultaneously: the transmission of probe, the FWM signals, and the fluorescence signals.

Considering the time-dependent Schrödinger equation, using a perturbation expansion and rotating wave approximation, we can obtain a series of density matrix equations as follows:

$$\frac{\partial}{\partial t}\rho_{00}^{(r)} = -\Gamma_{00}\rho_{00}^{(r)} + \mathrm{i}[G_1^*\rho_{10}^{(r-1)} - G_1\rho_{01}^{(r-1)}] \tag{1a}$$

$$\frac{\partial}{\partial t}\rho_{11}^{(r)} = -\Gamma_{11}\rho_{11}^{(r)} + \mathrm{i}[(G_1\rho_{01}^{(r-1)} - G_1^*\rho_{10}^{(r-1)}) + G_2^*(\rho_{21}^{(r-1)} - \rho_{12}^{(r-1)})] \tag{1b}$$

$$\frac{\partial}{\partial t}\rho_{10}^{(r)} = -(\mathrm{i}\Delta_1 + \Gamma_{10})\rho_{10}^{(r)} + \mathrm{i}[G_1(\rho_{00}^{(r-1)} - \rho_{11}^{(r-1)}) + G_2^*\rho_{20}^{(r-1)}] \tag{1c}$$

$$\frac{\partial}{\partial t}\rho_{20}^{(r)} = -[\mathrm{i}(\Delta_1 + \Delta_2) + \Gamma_{20}]\rho_{20}^{(r)} + \mathrm{i}[G_2^*\rho_{10}^{(r-1)} - G_1\rho_{21}^{(r-1)}] \tag{1d}$$

$$\frac{\partial}{\partial t}\rho_{21}^{(r)} = -(\mathrm{i}\Delta_2 + \Gamma_{21})\rho_{21}^{(r)} + \mathrm{i}[G_2(\rho_{11}^{(r-1)} - \rho_{22}^{(r-1)}) - G_1^*\rho_{20}^{(r-1)}] \tag{1e}$$

where G_1 and G_2 represents the Rabi frequencies of the laser filed E_1 and E_2 with $G_1 = \mu_{10}E_1/\hbar$ and $G_2 = \mu_{12}E_2/\hbar$, respectively, in which μ_{10} and μ_{12} are the electric dipole moment. In Eq. (1), Γ_{ij} is the decay rate between state $|i\rangle$ and $|j\rangle$ with the magnitude being 10^6 s^{-1} for the ^{85}Rb atomic system, and the subscript r is the order of nonlinearity. The susceptibility $\chi = \chi^{(1)} + \chi^{(3)}|E|^2$ can be calculated according to the relation $P = \varepsilon_0\chi E_p = N\mu_{10}\rho_{10}$ with N being the atomic density. By solving the Eq. (1), the susceptibility of the system under steady-state condition can be written as

$$\chi^{(1)} = \eta/K$$
$$\chi^{(3)}|E|^2 = \eta/K^2(|G_2|^2/d_2)$$

with $\eta = \mathrm{i}N\mu_{10}^2/(\hbar\varepsilon_0)$, $K = d_1 + |G_2|^2/d_2$, $d_1 = \Gamma_{10} + \mathrm{i}\Delta_1$, and $d_2 = \Gamma_{20} + \mathrm{i}(\Delta_1 + \Delta_2)$. Due to the inference of the dressing filed pair of E_2 and E_2', periodical dressing effect is offered $|G_2|^2 = G_2^2 + G_2'^2 + 2G_2G_2'\cos(2k_2z)$, which forms spatial periodic dressing pattern and a standing wave. Therefore, susceptibility χ composed of real part and imaginary part exhibits periodical behavior along with the$z$propagation direction, respectively depicted in Figs. 2(a) and (b). In this case, the susceptibility can be expressed as

$$\chi = \chi_0 + 2\sum_{n=1}^{\infty}\chi_n\cos[2nk_2\sin(\theta/2)z]$$

For a two-mode approximation, we solve for the first two Fourier coefficients of χ

$$\chi_0 = \mathrm{i}\frac{N\mu_{10}^2}{\varepsilon_0\hbar}\left[\frac{A}{\sqrt{1-B^2}} - \frac{C}{\sqrt{(1-B^2)^3}}\right] \tag{2a}$$

$$\chi_1 = \mathrm{i}\frac{N\mu_{10}^2}{\varepsilon_0\hbar}\left[A\frac{\sqrt{1-B^2}-1}{B\sqrt{1-B^2}} + \frac{BC}{\sqrt{(1-B^2)^3}}\right] \tag{2b}$$

where $A = d_2/(G_2^2 + G_2'^2 + d_1 d_2)$, $B = 2G_2G_2'/(G_2^2 + G_2'^2 + d_1 d_2)$ and $C = (G_2^2 + G_2'^2)d_2/(G_2^2 + G_2'^2 + d_1 d_2)^2$.

The plane-wave expansion method can be employed in the analysis of the photonic band gap (PBG) of the EIGs, readers can get more information in Ref. [16]. We obtain a general dispersion relationship of the EIG as

$$\kappa_\pm \approx k_1 \pm \frac{1}{2k_2\sin(\theta/2)} \cdot\sqrt{[k_1^2(1+\chi_0) - k_2^2\sin^2(\theta/2)]^2 - k_1^4\chi_1^2} \tag{3}$$

in which $\kappa_\pm$ is the Bloch wave number at the edge of Brillouin zone; The real part and imaginary part of Bloch wave number $\kappa_\pm$ with respect to the photonic band gap structures, correspondingly presented in Figs. 2(c) and (d), are obtained via scanning Δ_1 with θ set at π.

The PBG width connects tightly with the term under the square root in Eq. (3). The necessary but not sufficient condition is $[k_1^2(1+\chi_0) - k_2^2]^2 - k_1^4\chi_1^2 \leqslant 0$. Thus, we end up with the following formula,

$$\Delta_{\mathrm{gap}} = \frac{(\Delta_1 + \Omega_{10})[2 + 2\mathrm{Re}(\chi_0) + \mathrm{Re}(\chi_1)]}{2\sqrt{1+\mathrm{Re}(\chi_0)}\left[1 + \frac{1}{2}\left(\frac{\mathrm{Im}(\chi_0)}{1+\mathrm{Re}(\chi_0)}\right)^2\right]} \tag{4}$$

If we introduce the substitutions $\omega_0 = \Delta_1 + \Omega_{10}$ and $n_0 = \sqrt{1+\mathrm{Re}(\chi_0)}$, Eq. (4) can be rewritten as

$$\Delta_{\mathrm{gap}} = \frac{\omega_0 n_0^3[2n_0^2 + \mathrm{Re}(\chi_1)]}{2n_0^4 + \mathrm{Im}^2(\chi_0)} \tag{5}$$

by using which we can analyze the changing of EIT-type as well as electromagnetically induced absorption (EIA)-type PBG width.

Furthermore, two FWM nonlinear processes associated with E_{F1} and E_{F2} can occur between the energy levels $|0\rangle$ and $|1\rangle$, when the phase matching conditions $\boldsymbol{k}_{\mathrm{F1}} = \boldsymbol{k}_1 + \boldsymbol{k}_2 - \boldsymbol{k}_2'$ and $\boldsymbol{k}_{\mathrm{F2}} = \boldsymbol{k}_1 + \boldsymbol{k}_3 - \boldsymbol{k}_3'$ are fulfilled, respectively. In the former case, the density-matrix element $\rho_{10}^{(3)}$ of this FWM signal E_{F1} can be obtained via the perturbation chain (I): $\rho_{00}^{(0)} \xrightarrow{\omega_1} \rho_{10}^{(1)} \xrightarrow{\omega_2} \rho_{20}^{(2)} \xrightarrow{-\omega_2} \rho_{10}^{(3)}$, and the corresponding expression is: $\rho_{10\mathrm{F1}}^{(3)} = G_{\mathrm{F1}}/[(d_1 + |G_2|^2/d_2)^2 d_2]$, where $G_{\mathrm{F1}} = -\mathrm{i}G_1G_2(G_2')^*\exp(\mathrm{i}\boldsymbol{k}_{\mathrm{F1}}\cdot\boldsymbol{r})$. In the latter case, employing the perturbation chain (II): $\rho_{00}^{(0)} \xrightarrow{\omega_1} \rho_{10}^{(1)} \xrightarrow{-\omega_3} \rho_{30}^{(2)} \xrightarrow{\omega_3} \rho_{10}^{(3)}$, we can obtain the density-matrix element $\rho_{10}^{(3)}$ of E_{F2} and the expression is: $\rho_{10\mathrm{F2}}^{(3)} = G_{\mathrm{F2}}/[(d_1 + |G_2|^2/d_2)^2 d_3]$, where $G_{\mathrm{F2}} = -\mathrm{i}G_1G_3(G_3')^*\exp(\mathrm{i}\boldsymbol{k}_{\mathrm{F2}}\cdot\boldsymbol{r})$, $d_3 = \Gamma_{30} + \mathrm{i}(\Delta_1 - \Delta_3)$. However, the FWM ($E_{\mathrm{F2}}$) is not generated in the EIT window, so we can not consider it. In addition, two types of fluoresce signal falling into EIT window due to spontaneous emission are also obtained: the decay of photons from $|1\rangle$ to $|0\rangle$ generates single-photon fluoresce signal R_0 described by $\rho_{11}^{(2)} = -|G_1|^2/[\Gamma_{11}(d_1 + |G_2|^2/d_2)]$ (Liouville pathway $\rho_{00}^{(0)} \xrightarrow{G_1} \rho_{10}^{(1)} \xrightarrow{(G_1)^*} \rho_{11}^{(2)}$), and the decay of photons from $|2\rangle$ to $|1\rangle$ generates two-photon fluoresce signal R_1 with respect to $\rho_{22}^{(4)} = |G_1|^2|G_2|^2/[\Gamma_{22}d_1d_4(d_2 + |G_2|^2/d_1)]$ and $d_4 = \Gamma_{21} + \mathrm{i}\Delta_2$ (Liouville pathway $\rho_{00}^{(0)} \xrightarrow{G_1} \rho_{10}^{(1)} \xrightarrow{G_2} \rho_{20}^{(2)} \xrightarrow{(G_1)^*} \rho_{21}^{(3)} \xrightarrow{(G_2)^*} \rho_{22}^{(4)}$). For the probe transmission, the Liouville pathway is $\rho_{00}^{(0)} \xrightarrow{G_1} \rho_{10}^{(1)}$, and we can obtain the first-order density matrix element as $\rho_{10}^{(1)} = \mathrm{i}G_1/(d_1 + |G_2|^2/d_2)$.

Now, a conversation of energy can be obtained as $(I_{R0} + I_{R1} + I_{\mathrm{F}} + R + T)/I_{\mathrm{in}} = 1$, which reflects the energy flowing after the incidence of probe into the EIG. Indeed, the measured signal is composed of two process: one is enhanced nonlinear process due to the atomic coherence in EIT condition, which predominates in the observed signal. Besides, owing to the generated PBG structure, the probe beam E_1 is only able to 'travel' if their eigenvalue falls within an allowed band, and the reflected E_1

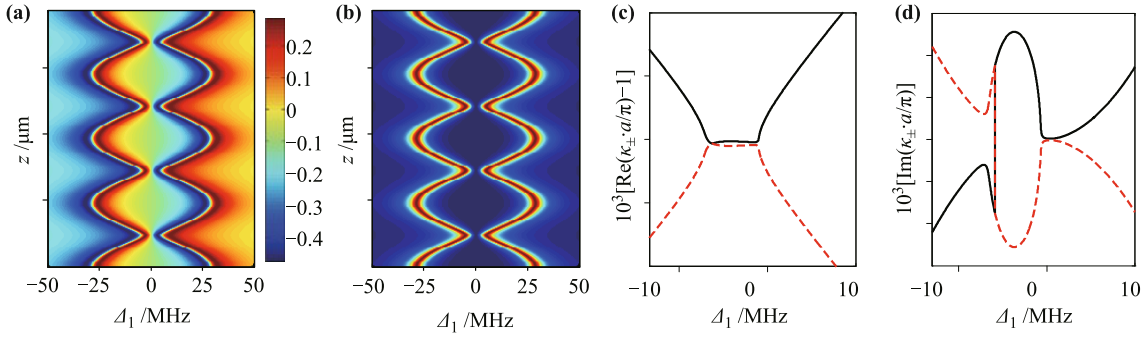

Fig. 2 **(a)** the real part and **(b)** the imaginary part of the compose susceptibility χ change with propagation z under the same color scale. In order to exhibit the changing trends, the amplitude is normalized. **(c, d)** The black-solid and red-dashed curves correspond to κ_+ and κ_- obtained from the Eq. (3).

can also result in nonlinear signal process. In angle and power controlled PBG, the reflection of incident probe beam E_1 is significantly modified, and therefore, we can observe transmitted probe, FWM, and fluoresce signal, which are effectively modulated.

3 Experimental results and analysis

In this section, we focus on the variation of the measured signals by discretely changing the relative angle α. In Fig. 3(a), the probe transmission [Fig. 3(a1)], FWM [Fig. 3(a2)] and fluoresce signal [Fig. 3(a3)] are depicted simultaneously, obtained by scanning Δ_2 with deflection angle α set at typical values. First, when the incident beam E_1 is vertically launched into the EIG ($\alpha = 0°$), EIT (peak higher than the baseline) appears at $\Delta_1 + \Delta_2 = 0$ in the probe transmission spectrum induced by $E_2(E_2')$ associated with the dressing trem $|E_2|^2/[\Gamma_{20}+\mathrm{i}(\Delta_1+\Delta_2)]$ when Δ_2 is scanned. Furthermore, relatively weak FWM signal E_{F1} and the two-photon fluoresce signal R_1, emerging as the peak on the background of single photon fluoresce signal R_0, are obtained due to enhanced nonlinear process. However, with α gradually varying from 0° to 0.4°, EIT becomes weak and finally disappears, displayed in the Fig. 3(a1), while the EIA (dip lower than the baseline) arises and becomes strong. The FWM and fluoresce signal R_1 are both significantly strengthened in company with the variation of the probe transmission spectrum, as shown in Figs. 3 (a2) and (a3), respectively.

Indeed, by adjusting α from bottom to top, the EIT gets weak, then completely disappears and switches into EIA, so that the PBG associated with them would also be affected. Taking the corresponding PBG [indicated by the black lines shown in Fig. 3(b)] into account, the width of PBG gradually increases along with α varying from 0° to 0.4°. As we know, if the PBG is wide enough and the electromagnetically induced Bragg reflection (EIBR) is big enough, the probe transmission spectrum changing in Fig. 3(a1) is reasonable. Especially, when the PBG width further increases to a certain value, the properties of probe transmission spectrum exhibit a peak to dip switch (EIT switch to EIA), which indicates more incident probe beam being reflected to generate E_{F1} and R_1. Note that as the α increases, lower dip of probe transmission emerges, resulting in a larger FWM and fluoresce signal due to the energy conversation. This explanation is in good agreement with the observation results of the FWM signal E_{F1} and two-photon fluoresce signal R_1, correspondingly depicted in the Figs. 3(a2) and (a3), which are obviously characterized by enhancement due to the enhanced EIBR compared with the result in such normal case $\alpha = 0°$.

In the section above, PBG modulated by angle α is reflected in the variation of signal's amplitude (probe transmission signal, FWM signal and fluoresce signal). Given that PBG width is determined by the Eq. (5), the power of dressing field can also affect the PBG width. In this section, we will address another intriguing aspect of our studies that power controlled PBG. In Fig. 4(a1), with Δ_1 fixed and P_2 at beginning, partial-EIA-partial-EIT appearing in the probe transmission spectrum versus Δ_2 can be observed due to the wide-narrow PBG structure, distinguished by whether it is lower and higher than the baseline. Moreover, through the term $|G_2|^2/d_2$ in $\rho_{10}^{(1)}$ when Δ_2 is scanned, we can obtain the corresponding bright state (EIA) is at $\Delta_1+\Delta_2|G_2|^2/|G_1|^2 = 0$ and dark state (EIT) at $\Delta_2 = 0$. In this case, the

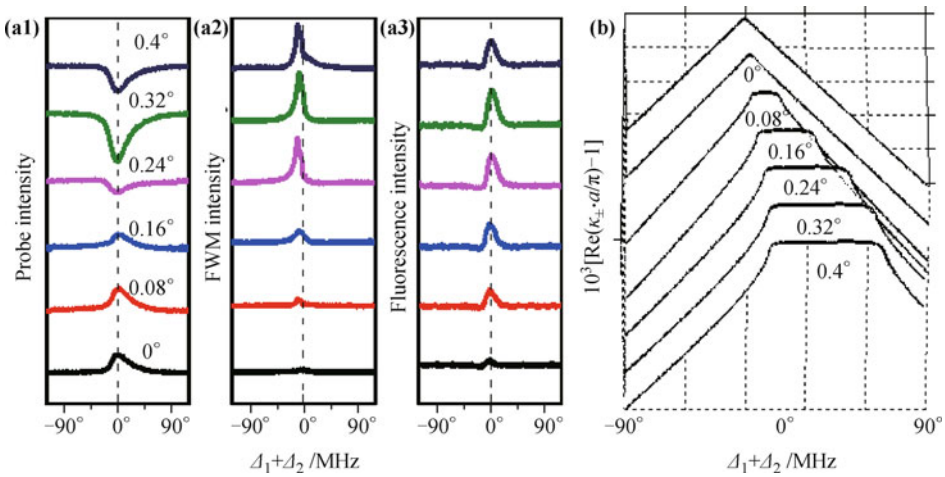

Fig. 3 **(a1–a3)** are probe transmission, FWM and fluorescence signals versus Δ_2 with α set at 0°, 0.08°, 0.16°, 0.24°, 0.32°, 0.4° from bottom to top. The other parameters are $P_1 = 3.6$ mW, $P_2 = 4.6$ mW, $P_2' = 5.4$ mW. **(b)** The theoretical PBG corresponding to (a1)–(a3).

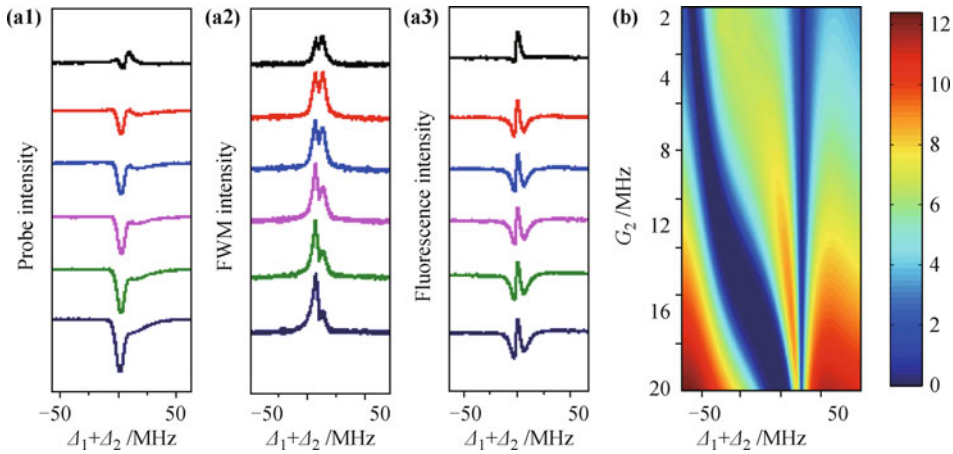

Fig. 4 **(a1–a3)** are probe transmission, FWM and fluorescence signals versus Δ_2 with increasing $P_2 = 6$, 8, 12, 16 and 20mW from top to bottom, when $P_1 = 4$ mW and $P_2' = 8$ mW. **(b)** The theoretical PBG corresponding to (a1)–(a3).

double structure PBG is depicted in Fig. 4(b), in which the wider one is EIA-type PBG, rather than EIT-type PBG. With P_2 increasing, the left dip of probe transmission becomes lower while the height of right peak decreases. Further increasing P_2, the dip becomes wider and deeper, and the peak nearly disappears. The reason is that the width of EIA-type increases with P_2, which generates more leftward probe transmission Bragg reflection. Finally, the probe transmission only shows one wide dip (EIA). The corresponding FWM is described in Fig. 4(a2). First, the main peak is caused by the two-photon emission term $\Gamma_{20} + \mathrm{i}(\Delta_1 + \Delta_2)$ and the suppression dip on the main peak is due to the two-photon resonance caused by the dressing term $|G_2|^2/[\Gamma_{20} + \mathrm{i}(\Delta_1 + \Delta_2)]$ in the expression of $\rho^{(3)}_{10\mathrm{F1}}$. Therefore, we can get similar-AT splitting versus Δ_2 as shown in Fig. 4(a2). Due to PBG associated with P_2 [Eq. (5)], the width of wide (narrow) PBG increases (decreases) gradually by increasing P_2, as shown in Fig. 4(b). As discussion above, the wider PBG, the more probe transmission is reflected to generate E_{F1}. Therefore, the left peak of E_{F1} increases rapidly with P_2.

The fluoresce signal in Fig. 4(a3) includes the dressed single-photon fluorescence R_0, suppressed by $E_2(E_2')$, depicted as the dip on each curve, and the sharp peak within each dip represents the emission of the two-photon fluorescence R_1. It is obvious in Fig. 4(a3) that the suppression dip of R_0 associated with the term $|G_2|^2/[\Gamma_{20} + \mathrm{i}(\Delta_1 + \Delta_2)]$ gets much deeper when P_2 increases from top to bottom. In addition, we notice that the height of fluorescence R_1 increases resulting from the wider PBG as discussed above.

4 Conclusion

In summary, we have experimentally investigated the enhancement of the FWM signal by the EIG induced by two non-collinear coupling beams. The PBG is modulated by changing the incident angle of probe beam and power of coupling laser beams. The intensities of probe transmission, FWM signal and fluoresce signal variation are investigated both in experiment and theory, and they agree with each other very well.

Acknowledgements This work was supported by China Postdoctoral Science Foundation (Grant No. 2012M521773), the National Natural Science Foundation of China (Grant Nos. 61308015, 61078002, 61078020, 11104214, and 61205112), and Xi'an Science and Technology Program (Grant Nos. CX12189WL02 and CX12189WL03).

References

1. K. J. Boller, A. Imamolu, and S. E. Harris, Observation of electromagnetically induced transparency, *Phys. Rev. Lett.*, 1991, 66(20): 2593
2. J. Gea-Banacloche, Y. Li, S. Jin, and M. Xiao, Electromagnetically induced transparency in ladder-type inhomogeneously broadened media: Theory and experiment, *Phys. Rev. A*, 1995, 51(1): 576
3. H. Kang, G. Hernandez, and Y. Zhu, Resonant four-wave mixing with slow light, *Phys. Rev. A*, 2004, 70(6): 061804 (R)
4. M. D. Lukin, A. B. Matsko, M. Fleischhauer, and M. O. Scully, Quantum noise and correlations in resonantly enhanced wave mixing based on atomic coherence, *Phys. Rev. Lett.*, 1999, 82(9): 1847
5. P. R. Hemmer, D. P. Katz, J. Donoghue, M. Cronin-Golomb, M. S. Shahriar, and P. Kumar, Efficient low intensity optical phase conjugation based on coherent population trapping in sodium, *Opt. Lett.*, 1995, 20(9): 982
6. M. Jain, H. Xia, G. Y. Yin, A. J. Merriam, and S. E. Harris, Efficient nonlinear frequency conversion with maximal

atomic coherence, *Phys. Rev. Lett.*, 1996, 77(21): 4326

7. M. Artoni and G. C. La Rocca, Optically tunable photonic stop bands in homogeneous absorbing media, *Phys. Rev. Lett.*, 2006, 96(7): 073905
8. J. W. Gao, Y. Zhang, N. Ba, C. L. Cui, and J. H. Wu, Dynamically induced double photonic bandgaps in the presence of spontaneously generated coherence, *Opt. Lett.*, 2010, 35(5): 709
9. Z. K. Wu, Y. Q. Zhang, T. K. Liu, Z. Y. Zhang, C. Li, Y. P. Zhang, and M. Xiao, Coherent control of dressed images of four-wave mixing, *Front. Phys.*, 2013, 8(2): 228
10. Y. P. Zhang, C. Z. Yuan, Y. Q. Zhang, H. B. Zheng, C. B. Li, Z. G. Wang, and M. Xiao, Surface solitons of four-wave mixing in an electromagnetically induced lattice, *Laser Phys. Lett.*, 2013, 10(5): 055406
11. Z. G. Wang, P. Ying, P. Y. Li, H. Y. Lan, H. Q. Huang, H. Tian, J. P. Song, and Y. P. Zhang, Phase regulated suppression and enhancement switches of four-wave mixing and fluorescence, *Front. Phys.*, 2014, 9(2): 153
12. A. Imamolu and S. E. Harris, Lasres without inversion: Interference of dressed lifetime-broadened state, *Opt. Lett.*, 1989, 14(24): 1344
13. G. Wang, H. Lu, and X. Liu, Dispersionless slow light in MIM waveguide based on a plasmonic analogue of electromagnetically induced transparency, *Opt. Exp.*, 2012, 20: 902
14. C. Liu, Z. Dutton, C. Behroozi, and L. Hau, Controlling photons using electromagnetically induced transparency, *Nature*, 2001, 409: 490
15. X. Liu, X. Yang, F. Lu, J. Ng, X. Zhou, and C. Lu, Stable and uniform dual-wavelength erbium-doped fiber laser based on fiber Bragg gratings and photonic crystal fiber, *Opt. Exp.*, 2005, 13(1): 142
16. J. H. Wu, M. Artoni, and G. C. La Rocca, Controlling the photonic band structure of optically driven cold atoms, *J. Opt. Soc. Am. B*, 2008, 25(11): 1840